Quantum spin-flip model of vertical-cavity surface-emitting lasers

J.-P. Hermier,[1] M. I. Kolobov,[2] I. Maurin,[1] and E. Giacobino[1]
[1]*Laboratoire Kastler Brossel, Université Pierre et Marie Curie, F-75252 Paris Cedex 05, France*
[2]*Laboratoire PhLAM, Université de Lille 1, F-59655 Villeneuve d'Ascq Cedex, France*
(Received 28 November 2001; published 13 May 2002)

We present a theoretical and experimental investigation of quantum fluctuations in vertical-cavity surface-emitting lasers (VCSELs) having one longitudinal and transverse linearly polarized mode above threshold. We develop the quantum version of the broadly used four-level spin-flip model to take into account the quantum statistics of the pumping process of the active atoms. Our theory allows for arbitrary pumping statistics varying from Poissonian to regular. We compare experimental results obtained with single-mode VCSELs with predictions of our theory and find very good agreement. We demonstrate that the quantum fluctuations of the subthreshold field component polarized orthogonally to the lasing mode have to be taken into account for adequate description of quantum fluctuations in VCSELs. In particular, we show that when the laser light passes through a polarizer, the two orthogonal polarization components of the light wave after passing through the polarizer can be strongly anticorrelated.

DOI: 10.1103/PhysRevA.65.053825 PACS number(s): 42.50.Lc, 42.50.Ct, 42.55.Px

I. INTRODUCTION

Ventral-cavity surface-emitting lasers (VCSELs) have been studied in detail the latest years because of several interesting characteristics that make them very attractive for applications, such as in optical telecommunications. They have a high quantum efficiency, a very low threshold, and can operate with only one longitudinal and transverse mode above threshold. As these features suggest, these lasers are very good candidates for squeezed light generation, i.e., decreasing the intensity noise below the standard quantum limit, by applying the pump noise suppression principle [1,2]. Presently, squeezing in VCSELs has been demonstrated experimentally for both single-mode operation and in a multi-transverse-mode regime [3,4]. For very high rate optical telecommunication in the range of several GHz [5], squeezing is of great importance for improving the bit-error rate.

In general, single-mode operation is more suitable for generating squeezed light. However, as the driving current increases other transverse modes start to oscillate [6,7] resulting in a multi-transverse-mode regime. In addition to this complication, VCSELs are known to present an unstable behavior, such as polarization switching [8–10] between different polarization modes. In applications, if polarization sensitive elements are used, this behavior can deteriorate the signal-to-noise ratio and lead to an increase of the intensity noise destroying squeezing. Hence, a proper understanding of polarization fluctuations in VCSELs is important for fundamental reasons as well as for applications.

In single-mode operation with only one linearly polarized mode above threshold it has already been pointed out that the fluctuations in a subthreshold mode with polarization orthogonal to the lasing mode can present a large intensity noise (one can directly measure it with a simple photodiode because this noise is far above the electronical dark noise). A semiclassical model was developed and showed that the intensity fluctuations in the subthreshold mode can be highly correlated with the intensity fluctuations of the oscillating mode [11–13]. This phenomenon is analogous to the multimode effects observed in standard laser diodes [14–16]. For these semiconductor lasers, the longitudinal mode above threshold has intensity fluctuations strongly anticorrelated with intensity fluctuations of the other longitudinal modes below threshold. For VCSELs the anticorrelations between transverse modes above threshold have also been studied [4,17–20].

The aim of our paper is to investigate in detail theoretically as well as experimentally the quantum fluctuations of VCSELs in the single-mode operation regime. Let us point out that in the case of our VCSELs the fluctuations in a subthreshold mode with polarization orthogonal to the lasing mode is very weak (comparable with the electronical dark noise). Since quantum effects are concerned, we have developed a quantum theory of fluctuations in this type of lasers based on the well-known spin-flip model first proposed by San Miguel, Feng, and Moloney [21], and broadly used for description of polarization dynamics of VCSELs. In Secs. II-IV, we describe in detail the full quantum spin-flip model of VCSELs. Our quantum description takes into account the pump statistics of the active laser medium, which we allow to vary from Poissonian to completely regular one. In Sec. V we discuss the theoretical predictions of our model. We demonstrate that taking into account the quantum fluctuations of both polarization components of the electromagnetic field, one above and another below threshold, is crucial for correct description of the quantum fluctuations of light emitted by these type of lasers. In Sec. VI we present our experimental results and compare them with predictions of our theory. The agreement is found to be very good. In Sec. VII we summarize the results of our work.

II. QUANTUM HEISENBERG-LANGEVIN EQUATIONS

We shall present here the quantum version of the classical four-level spin-flip model of VCSELs developed by San Miguel, Feng, and Moloney [21]. This model describes very well the dynamics of these semiconductor lasers and is

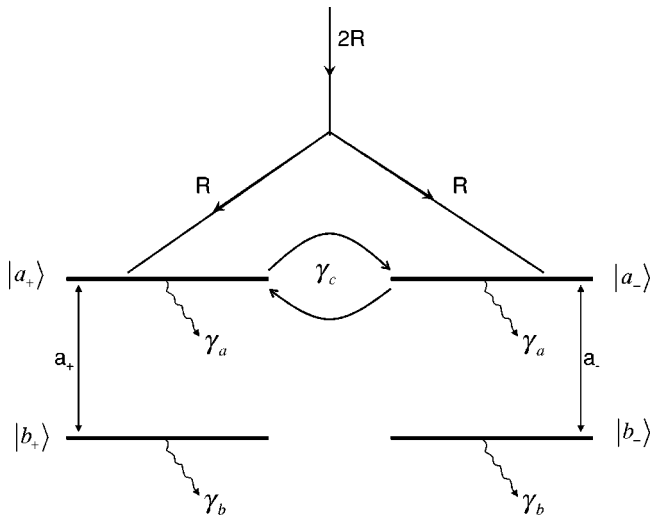

FIG. 1. Four-level scheme of the active medium.

widely used for understanding of such phenomena, for example, as polarization switching. The spin-flip model takes into account the spin sublevels of the total angular momentum of the heavy holes in the valence band and of the electrons in the conduction band. These four sublevels interact with two circularly polarized electromagnetic waves in the laser resonator and it is this interaction that is responsible for the complicated polarization dynamics manifested by these types of lasers.

The four-level scheme of the semiconductor medium is shown in Fig. 1. Two lower levels $|b\pm\rangle$ correspond to the unexcited state of the semiconductor medium with zero electron-hole pairs while the upper levels $|a\pm\rangle$ to the excited states with an electron-hole pair created [22]. Two pairs of levels $|a+\rangle,|b+\rangle$ and $|a-\rangle,|b-\rangle$ are coupled via interaction with the left and right circularly polarized electromagnetic waves in the laser cavity described by the field operators $a_+(t)$ and $a_-(t)$. As explained in Ref. [21], physically these two pairs of transitions are associated with two z components $J_z=\pm 1/2$ of the total angular momentum $J=1/2$ of the electrons in the conduction band and corresponding z components $J_z=\pm 3/2$ for $J=3/2$ of the heavy holes in the valence band.

We consider a semiconductor medium that fills a cavity of length L, volume V with an intensity transmission coefficient of the coupling mirrors T. We assume that the finesse of the cavity is high enough to neglect the spatial variations of the electromagnetic field (the mean-field approximation). We also consider the two circularly polarized light waves as traveling plane waves of frequency ω resonant with the cavity frequency.

Since in our experiments we use the technique of the pump-noise suppression [1,2], we have to incorporate in our quantum model the possibility of varying the pump statistics of the active laser medium. We shall follow the method used to describe the pump statistics in three-level lasers [23–25]. In this description the random excitation of the atoms is mimicked by injection of excited atoms into the laser cavity at random time moments t_j. The pump statistics thus corresponds to the statistics of these times t_j. As shown in Ref. [23], for stationary in-time average pumping rate, the influence of the pump statistics can be characterized by a single parameter $p, 0\leqslant p\leqslant 1$. For $p=1$, the pump is perfectly regular while for $p=0$ the pump has Poissonian statistics. The difference of our situation from the model considered in Refs. [23–25] is that we have two excited levels $|a+\rangle$ and $|a-\rangle$, which are pumped together by an electric current with varying statistics (see Fig. 1). Therefore, we have to take into account the statistics of partition between two sublevels $|a+\rangle$ and $|a-\rangle$.

We assume that the jth carrier described by our four-level scheme is created in the laser cavity at time t_j and from this moment starts to interact with a single cavity mode. This interaction is described by the following Heisenberg-Langevin equations:

$$\frac{d}{dt}\hat{a}_\pm(t)=-\kappa\hat{a}_\pm(t)-i\omega_p\hat{a}_\mp(t) - ig\sum_j \theta(t-t_j)\hat{\sigma}^j_\pm(t)+\hat{f}_\pm(t), \tag{2.1}$$

$$\frac{d}{dt}\hat{\sigma}^j_\pm(t)=-\gamma_\perp(1+i\alpha)\hat{\sigma}^j_\pm(t)+ig\,\theta(t-t_j) \times[\hat{\sigma}^j_{a\pm}(t)-\hat{\sigma}^j_{b\pm}(t)]\hat{a}_\pm(t)+\hat{f}^j_{\sigma\pm}(t), \tag{2.2}$$

$$\frac{d}{dt}\hat{\sigma}^j_{a\pm}(t)=-\gamma_a\hat{\sigma}^j_{a\pm}(t)-\gamma_c[\hat{\sigma}^j_{a\pm}(t)-\hat{\sigma}^j_{a\mp}(t)]-ig\,\theta(t-t_j) \times[\hat{a}_\pm(t)\hat{\sigma}^{j\dagger}_\pm(t)-\hat{a}^\dagger_\pm(t)\hat{\sigma}^j_\pm(t)]+\hat{f}^j_{a\pm}(t), \tag{2.3}$$

$$\frac{d}{dt}\hat{\sigma}^j_{b\pm}(t)=-\gamma_b\hat{\sigma}^j_{b\pm}(t)+ig\,\theta(t-t_j)[\hat{a}_\pm(t)\hat{\sigma}^{j\dagger}_\pm(t) -\hat{a}^\dagger_\pm(t)\hat{\sigma}^j_\pm(t)]+\hat{f}^j_{b\pm}(t), \tag{2.4}$$

where $\hat{\sigma}^j_{a\pm}=(|a\pm\rangle\langle a\pm|)^j$ and $\hat{\sigma}^j_{b\pm}=(|b\pm\rangle\langle b\pm|)^j$ are the projection operators on the upper and lower levels of our scheme, $\hat{\sigma}^j_\pm(t)$ are the spin-flip operators in the frame rotating at frequency ω, which represent the complex polarization of the jth carrier, and $\hat{a}_+(t)$ and $\hat{a}_-(t)$ are the photon annihilation operators for the laser mode with right and left circular polarization. The operators $\hat{f}_\pm(t)$, and $\hat{f}^j_{\alpha\pm}(t)$ with $\alpha=\sigma,a,b$ are the operator-valued microscopic Langevin forces that guarantee the conservation of the commutation relations for the corresponding atomic and field operators, $\theta(t)$ is the step function, and κ is the cavity damping constant,

$$\kappa=\frac{cT}{2nL}, \tag{2.5}$$

where n is the refractive index of the semiconductor medium. The constants γ_a and γ_b are the decay rates of the populations of the upper and lower levels, $\gamma_\perp$ is the decay rate of the polarization, and γ_c is the intraband relaxation rate. The last parameter was introduced in Ref. [21] to de-

scribe the spin-flip relaxation process. This parameter is responsible for coupling of the two transitions with different polarizations and, consequently, for nontrivial polarization dynamics of VCSELs. Next, ω_p describes the linear birefringence, and the coupling constant g is given by

$$g=\nu\mu\sqrt{\frac{1}{2\hbar\epsilon_0\omega V}}, \tag{2.6}$$

where μ is the magnitude of the dipole moment and ν the frequency associated with the energy gap; α is the standard linewidth enhancement of the semiconductor-laser theory,

$$\alpha=\frac{\nu-\omega}{\gamma_\perp}. \tag{2.7}$$

The Langevin forces $\hat{f}_\pm(t)$, and $\hat{f}^j_{\alpha\pm}(t)$ are fully characterized by their first- and second-order moments. The only nonzero normally ordered correlation functions of the Langevin forces $\hat{f}_\pm(t)$ are equal to

$$\langle\hat{f}^\dagger_\pm(t)\hat{f}_\pm(t')\rangle=2\kappa\overline{n_T}\delta(t-t'). \tag{2.8}$$

Here $\overline{n_T}$ is the mean number of thermal photons at temperature T. For optical frequencies this quantity is negligibly small and in what follows we will neglect it assuming that the reservoir is at zero temperature, $T=0$. Since in this case all the normally ordered correlation functions of $\hat{f}_\pm(t)$ vanish, we can put $\hat{f}_\pm(t)=0$.

The correlation functions of the Langevin forces $\hat{f}^j_{\alpha\pm}(t)$ can be calculated, for example, using the Einstein relation [25]. For completeness we give here the nonzero correlation functions of these forces:

$$\langle\hat{f}^j_{a\pm}(t)\hat{f}^j_{a\pm}(t')\rangle=[\gamma_a\langle\hat{\sigma}^j_{a\pm}(t)\rangle+\gamma_c(\langle\hat{\sigma}^j_{a\pm}(t)\rangle+\langle\hat{\sigma}^j_{a\mp}(t)\rangle)]\delta(t-t'), \tag{2.9}$$

$$\langle\hat{f}^j_{a\pm}(t)\hat{f}^j_{a\mp}(t')\rangle=-\gamma_c(\langle\hat{\sigma}^j_{a\pm}(t)\rangle+\langle\hat{\sigma}^j_{a\mp}(t)\rangle)\delta(t-t'), \tag{2.10}$$

$$\langle\hat{f}^j_{b\pm}(t)\hat{f}^j_{b\pm}(t')\rangle=\gamma_b\langle\hat{\sigma}^j_{b\pm}(t)\rangle\delta(t-t'), \tag{2.11}$$

$$\langle\hat{f}^{\dagger j}_{\sigma\pm}(t)\hat{f}^j_{\sigma\pm}(t')\rangle=[(2\gamma_\perp-\gamma_a-\gamma_c)\langle\hat{\sigma}^j_{a\pm}(t)\rangle+\gamma_c\langle\hat{\sigma}^j_{a\mp}(t)\rangle]\delta(t-t'), \tag{2.12}$$

$$\langle\hat{f}^j_{\sigma\pm}(t)\hat{f}^{\dagger j}_{\sigma\pm}(t')\rangle=(2\gamma_\perp-\gamma_b)\langle\hat{\sigma}^j_{b\pm}(t)\rangle\delta(t-t'), \tag{2.13}$$

$$\langle\hat{f}^j_{\sigma\pm}(t)\hat{f}^j_{a\pm}(t')\rangle=(\gamma_a+\gamma_c)\langle\hat{\sigma}^j_{\pm}(t)\rangle\delta(t-t'), \tag{2.14}$$

$$\langle\hat{f}^j_{\sigma\pm}(t)\hat{f}^j_{a\mp}(t')\rangle=-\gamma_c\langle\hat{\sigma}^j_{\pm}(t)\rangle\delta(t-t'), \tag{2.15}$$

$$\langle\hat{f}^{\dagger j}_{\sigma\pm}(t)\hat{f}^j_{b\pm}(t')\rangle=\gamma_b\langle\hat{\sigma}^{\dagger j}_{\pm}(t)\rangle\delta(t-t'). \tag{2.16}$$

To take into account the pumping statistics of the active medium of the VCSEL we shall use the same strategy as in Ref. [24] and define the following collective operators that incorporate the random arrivals of the carriers into the cavity,

$$\hat{N}_{a\pm}(t)=\sum_j\ \theta(t-t_j)\hat{\sigma}^j_{a\pm}(t), \tag{2.17}$$

$$\hat{N}_{b\pm}(t)=\sum_j\ \theta(t-t_j)\hat{\sigma}^j_{b\pm}(t), \tag{2.18}$$

for the collective populations, and

$$\hat{P}_\pm(t)=-i\sum_j\ \theta(t-t_j)\hat{\sigma}^j_{\pm}(t), \tag{2.19}$$

for the collective polarization. The additional factor $-i$ in Eq. (2.19) is introduced for mathematical convenience. To calculate the correlation functions of these macroscopic operators we have to perform two averages, the quantum average and the classical average over the arrival times t_j. This last average accounts for the pumping statistics of the active medium.

The Heisenberg-Langevin equations for collective operators (2.17)–(2.19) are obtained by taking the temporal derivative of these operators and using Eqs. (2.1)–(2.4) for individual operators. For example, for $\hat{N}_{a\pm}(t)$ we have

$$\begin{aligned}\frac{d}{dt}\hat{N}_{a\pm}(t)&=\sum_j\left[\delta(t-t_j)\hat{\sigma}^j_{a\pm}(t)+\theta(t-t_j)\frac{d}{dt}\hat{\sigma}^j_{a\pm}(t)\right]\\&=\sum_j\ \delta(t-t_j)\hat{\sigma}^j_{a\pm}(t)-\gamma_a\hat{N}_{a\pm}(t)\\&\quad-\gamma_c[\hat{N}_{a\pm}(t)-\hat{N}_{a\mp}(t)]-g[\hat{a}^\dagger_\pm(t)\hat{P}_\pm(t)\\&\quad+\hat{a}_\pm(t)\hat{P}^\dagger_\pm(t)]\\&\quad+\sum_j\ \theta(t-t_j)\hat{f}^j_{a\pm}(t).\end{aligned} \tag{2.20}$$

The first term in the right-hand side of Eq. (2.20) corresponds to the random arrivals of the carriers into the cavity. This is easy to see if we calculate its expectation value,

$$\begin{aligned}\left\langle\sum_j\ \delta(t-t_j)\hat{\sigma}^j_{a\pm}(t)\right\rangle&=\left\langle\sum_j\ \delta(t-t_j)\langle\hat{\sigma}^j_{a\pm}(t)\rangle\right\rangle_S\\&=\frac{1}{2}\left\langle\sum_j\ \delta(t-t_j)\right\rangle_S.\end{aligned} \tag{2.21}$$

Here we have taken the double averaging, the first over the quantum state of the carriers and the second, indicated by index S over the classical statistics of arrival times t_j. For calculation of the quantum-mechanical mean value we have used the fact that when the carriers arrive into the cavity, they are with equal probability of 1/2 in the state $|a+\rangle$ or $|a-\rangle$ so that $\langle\hat{\sigma}^j_{a\pm}(t_j)\rangle=1/2$. The last expression in Eq.

(2.21) indicates the average over the classical arrival statistics and, for stationary pumping process, yields the mean pumping rate,

$$\left\langle \sum_j \delta(t-t_j) \right\rangle_S = 2R \int_{-\infty}^{+\infty} dt_j \delta(t-t_j) = 2R. \quad (2.22)$$

The mean pumping rate R is related to each upper level $|a+\rangle$ or $|a-\rangle$, so that the total mean pumping rate of both levels is $2R$. Equations for the collective populations $\hat{N}_{a\pm}(t)$ can now be written as

$$\frac{d}{dt}\hat{N}_{a\pm}(t) = R - \gamma_a \hat{N}_{a\pm}(t) - \gamma_c[\hat{N}_{a\pm}(t) - \hat{N}_{a\mp}(t)] - g[\hat{a}^\dagger_\pm(t)\hat{P}_\pm(t) + \hat{a}_\pm(t)\hat{P}^\dagger_\pm(t)] + \hat{F}_{a\pm}(t), \quad (2.23)$$

with the collective Langevin forces $\hat{F}_{a\pm}(t)$ equal to

$$\hat{F}_{a\pm}(t) = \sum_j \delta(t-t_j)\hat{\sigma}^j_{a\pm}(t) + \sum_j \theta(t-t_j)\hat{f}^j_{a\pm}(t) - R. \quad (2.24)$$

Equations for the other collective operators can be obtained in the same way and give the following results:

$$\frac{d}{dt}\hat{a}_\pm(t) = -\kappa\hat{a}_\pm(t) - i\omega_p\hat{a}_\mp(t) + g\hat{P}_\pm(t), \quad (2.25)$$

$$\frac{d}{dt}\hat{P}_\pm(t) = -\gamma_\perp(1+i\alpha)\hat{P}_\pm(t) + g[\hat{N}_{a_\pm}(t) - \hat{N}_{b_\pm}(t)] \times \hat{a}_\pm(t) + \hat{f}_{P\pm}(t), \quad (2.26)$$

$$\frac{d}{dt}\hat{N}_{b\pm}(t) = -\gamma_b\hat{N}_{b\pm}(t) + g[\hat{a}^\dagger_\pm(t)\hat{P}_\pm(t) + \hat{a}_\pm(t)\hat{P}^\dagger_\pm(t)] + \hat{f}_{b\pm}(t). \quad (2.27)$$

The Langevin forces $\hat{F}_{P\pm}(t)$ and $\hat{F}_{b\pm}(t)$ read

$$\hat{F}_{P\pm}(t) = \sum_j \delta(t-t_j)\hat{\sigma}^j_\pm(t) + \sum_j \theta(t-t_j)\hat{f}^j_{\sigma\pm}(t), \quad (2.28)$$

$$\hat{F}_{b\pm}(t) = \sum_j \delta(t-t_j)\hat{\sigma}_{b\pm}(t) + \sum_j \theta(t-t_j)\hat{f}^j_{b\pm}(t). \quad (2.29)$$

The correlation functions of the collective Langevin forces $\hat{F}_{a\pm}(t)$,$\hat{F}_{b\pm}(t)$, and $\hat{F}_{P\pm}(t)$ can be evaluated in the same way as in Ref. [23]. A new element that appears in calculation of these correlation functions is the repartition of carriers in two sublevels $|a+\rangle$ and $|a-\rangle$ according to the Poissonian statistics with an equal probability of 1/2. We omit here the calculations and give directly the correlation functions of the collective Langevin forces,

$$\langle \hat{F}_{a\pm}(t)\hat{F}_{a\pm}(t')\rangle = [\gamma_a\langle\hat{N}_{a\pm}(t)\rangle + \gamma_c(\langle\hat{N}_{a\pm}(t)\rangle + \langle\hat{N}_{a\mp}(t)\rangle) + R(1-p/2)]\delta(t-t'), \quad (2.30)$$

$$\langle \hat{F}_{a\pm}(t)\hat{F}_{a\mp}(t')\rangle = [-\gamma_c(\langle\hat{N}_{a\pm}(t)\rangle + \langle\hat{N}_{a\mp}(t)\rangle) - pR/2] \times \delta(t-t'), \quad (2.31)$$

$$\langle \hat{F}_{b\pm}(t)\hat{F}_{b\pm}(t')\rangle = \gamma_b\langle\hat{N}_{b\pm}(t)\rangle\delta(t-t'), \quad (2.32)$$

$$\langle \hat{F}^\dagger_{P\pm}(t)\hat{F}_{P\pm}(t')\rangle = [(2\gamma_\perp - \gamma_a - \gamma_c)\langle\hat{N}_{a\pm}(t)\rangle + \gamma_c\langle\hat{N}_{a\mp}(t)\rangle + R]\delta(t-t'), \quad (2.33)$$

$$\langle \hat{F}_{P\pm}(t)\hat{F}^\dagger_{P\pm}(t')\rangle = (2\gamma_\perp - \gamma_b)\langle\hat{N}_{b\pm}(t)\rangle\delta(t-t'), \quad (2.34)$$

$$\langle \hat{F}_{P\pm}(t)\hat{F}_{a\pm}(t')\rangle = (\gamma_a + \gamma_c)\langle\hat{P}_\pm(t)\rangle\delta(t-t'), \quad (2.35)$$

$$\langle \hat{F}_{P\pm}(t)\hat{F}_{a\mp}(t')\rangle = -\gamma_c\langle\hat{P}_\pm(t)\rangle\delta(t-t'), \quad (2.36)$$

$$\langle \hat{F}^\dagger_{P\pm}(t)\hat{F}_{b\pm}(t')\rangle = \gamma_b\langle\hat{P}^\dagger_\pm(t)\rangle\delta(t-t'). \quad (2.37)$$

As follows from these correlation functions, the parameter p that determines the pumping statistics of the active medium, appears in the first two correlation functions, related to the populations of the upper levels $|a+\rangle$ and $|a-\rangle$. Let us remind that $p=0$ corresponds to the completely regular statistics of the total pumping rate $2R$. However, since the carriers arriving regularly with the rate $2R$ are randomly distributed between two levels $|a+\rangle$ and $|a-\rangle$, the random statistics is partially recovered because of the partition noise. This is the reason why the parameter p in the first two correlation functions appears with the factor 1/2. Therefore, one can never have the completely regular pumping statistics of the individual levels $|a+\rangle$ and $|a-\rangle$.

III. *c*-NUMBER STOCHASTIC LANGEVIN EQUATIONS

Now we shall derive the *c*-number Langevin equations corresponding to the Eqs. (2.23) and (2.25)–(2.27). For this, we have to choose an order for products of atomic and field operators. Indeed, *c*-number variables commute while the operators do not. Therefore, we obtain a unique relationship between the operators and the *c*-number variables only if we define the correspondence between a product of operators and a product of the corresponding *c*-number variables. We choose as in Refs. [23–25], the normal order of atomic and field operators:

$$\hat{a}^\dagger_\pm, \hat{P}^\dagger_\pm, \hat{N}_{a\pm}, \hat{N}_{b\pm}, \hat{P}_\pm, \hat{a}_\pm. \quad (3.1)$$

For *c*-number variables we shall use the same letters as for operators but without hats. Equations for the *c* numbers are easily obtained from equations for the operators since the latter are already written in the normal ordering:

$$\dot{a}_{\pm}(t) = -\kappa a_{\pm}(t) - i\omega_p a_{\mp}(t) g P_{\pm}(t), \tag{3.2}$$

$$\dot{P}_{\pm}(t) = -\gamma_{\perp}(1+i\alpha)P_{\pm}(t) + g[N_{a\pm}(t) - N_{b\pm}(t)]a_{\pm}(t) + F_{P\pm}(t), \tag{3.3}$$

$$\dot{N}_{a\pm}(t) = R - \gamma_a N_{a\pm}(t) - \gamma_c[N_{a\pm}(t) - N_{a\mp}(t)] - g[a^*_{\pm}(t)P_{\pm}(t) + a_{\pm}(t)P^*_{\pm}(t)] + F_{a\pm}(t), \tag{3.4}$$

$$\dot{N}_{b\pm}(t) = -\gamma_b N_{b\pm}(t) + g[a^*_{\pm}(t)P_{\pm}(t) + a_{\pm}(t)P^*_{\pm}(t)] + F_{b\pm}(t). \tag{3.5}$$

Correlation functions of the *c*-number Langevin forces in these equations are different from the correlation functions of the corresponding operator-valued forces in Eqs. (2.30)–(2.37). They are calculated from the requirement that the *c*-number equations for the second moments are identical to the corresponding normally ordered operator equations. After straightforward calculations, we obtain the following nonzero correlation functions:

$$\langle F_{a\pm}(t)F_{a\pm}(t')\rangle = [\gamma_a\langle N_{a\pm}(t)\rangle + \gamma_c(\langle N_{a\pm}(t)\rangle + \langle N_{a\mp}(t)\rangle) + R(1-p/2) - g\langle a^*_{\pm}(t)P_{\pm}(t) + a_{\pm}(t)P^*_{\pm}(t)\rangle]\delta(t-t'), \tag{3.6}$$

$$\langle F_{a\pm}(t)F_{a\mp}(t')\rangle = [-\gamma_c(\langle N_{a\pm}(t)\rangle + \langle N_{a\mp}(t)\rangle) - pR/2] \times \delta(t-t'), \tag{3.7}$$

$$\langle F_{a\pm}(t)F_{b\pm}(t')\rangle = g\langle a^*_{\pm}(t)P_{\pm}(t) + a_{\pm}(t)P^*_{\pm}(t)\rangle\delta(t-t'), \tag{3.8}$$

$$\langle F_{b\pm}(t)F_{b\pm}(t')\rangle = [\gamma_b\langle N_{b\pm}(t)\rangle - g\langle a^*_{\pm}(t)P_{\pm}(t) + a_{\pm}(t)P^*_{\pm}(t)\rangle]\delta(t-t'), \tag{3.9}$$

$$\langle F^*_{P\pm}(t)F_{P\pm}(t')\rangle = [(2\gamma_{\perp} - \gamma_a - \gamma_c)\langle N_{a\pm}(t)\rangle + \gamma_c\langle N_{a\mp}(t)\rangle + R]\delta(t-t'), \tag{3.10}$$

$$\langle F_{P\pm}(t)F_{P\pm}(t')\rangle = 2g\langle a_{\pm}(t)P_{\pm}(t)\rangle\delta(t-t'), \tag{3.11}$$

$$\langle F_{P\pm}(t)F_{b\pm}(t')\rangle = \gamma_b\langle P_{\pm}(t)\rangle\delta(t-t'). \tag{3.12}$$

Up to this moment we have kept the decay constants $\gamma_a, \gamma_b, \gamma_{\perp}$, and κ completely arbitrary. As mentioned in the literature (see, for example, Ref. [26]), for our model to describe a semiconductor laser we have to assume the decay rate γ_b of the lower level to be very large compared to all the other decay constants. This assumption allows us to adiabatically eliminate the populations $N_{b\pm}(t)$. Moreover, the relaxation rate $\gamma_{\perp}$ of polarization in VCSELs is much bigger that the relaxation rate γ_a. Therefore, the macroscopic polarizations $P_{\pm}(t)$ can also be adiabatically eliminated. These two adiabatic eliminations leave us with equations for the two upper populations $N_{a\pm}(t)$ and the two field components $a_{\pm}(t)$. Following the literature we shall introduce the new variables of the total carrier population $D(t) = [N_{a+}(t) + N_{a-}(t)]/2$ and the population difference $d(t) = [N_{a+}(t) - N_{a-}(t)]/2$. The equations for these variables and two field components are

$$\dot{a}_{\pm}(t) = -\kappa a_{\pm}(t) - i\omega_p a_{\mp}(t) + c(1-i\alpha) \times [D(t) \pm d(t)]a_{\pm}(t) + F_{\pm}(t), \tag{3.13}$$

$$\dot{D}(t) = R - \gamma D(t) - c(|a_+(t)|^2 + |a_-(t)|^2)D(t) - c(|a_+(t)|^2 - |a_-(t)|^2)d(t) + F_D(t), \tag{3.14}$$

$$\dot{d}(t) = -\gamma_s d(t) - c(|a_+(t)|^2 - |a_-(t)|^2)D(t) - c(|a_+(t)|^2 + |a_-(t)|^2)d(t) + F_d(t). \tag{3.15}$$

Here we have defined the spin-flip rate γ_s as $\gamma_s = \gamma_a + 2\gamma_c$ and have introduced the following shorthands:

$$c = \frac{g^2}{\gamma_{\perp}(1+\alpha^2)}, \qquad \gamma = \gamma_a. \tag{3.16}$$

The Langevin forces in Eqs. (3.13)–(3.15) are related to the Langevin forces in Eqs. (3.2)–(3.5) as follows:

$$F_{\pm}(t) = \frac{g(1-i\alpha)}{\gamma_{\perp}(1+\alpha^2)}\left[F_{P\pm}(t) - \frac{g}{\gamma_b}a_{\pm}(t)F_{b\pm}(t)\right], \tag{3.17}$$

$$F_D(t) = \frac{1}{2}[F_{a+}(t) + F_{a-}(t)] - \frac{1}{2}[a^*_{+}(t)F_{+}(t) + a^*_{-}(t)F_{-}(t) + \text{c.c.}], \tag{3.18}$$

$$F_d(t) = \frac{1}{2}[F_{a+}(t) - F_{a-}(t)] - \frac{1}{2}[a^*_{+}(t)F_{+}(t) - a^*_{-}(t)F_{-}(t) + \text{c.c.}]. \tag{3.19}$$

Calculation of the corresponding correlation functions using these equations is straightforward but tedious and the final results very cumbersome. Therefore, since we are interested in investigating the quantum fluctuations around the stationary solutions, we shall not give here these general results for the correlations functions but provide below more simple expressions valid for the stationary state of the VCSEL.

Equations (3.13)-(3.15) possess the solutions that can be written in the form

$$a_{\pm}(t) = Qe^{i(\Delta t \pm \psi)}, \quad D(t) = D_0, \quad d(t) = d_0, \tag{3.20}$$

and are called stationary solutions because they are characterized by constant values of the field amplitude Q and the atomic populations D_0 and d_0. The only time dependence in these solutions corresponds to the frequency shift Δ with respect to the resonator frequency ω. These stationary solu-

tions have been investigated in detail in Refs. [6,21]. We shall give here the summary of the results that we will need for investigation of the fluctuation properties of VCSELs.

First, let us consider the situation without birefringence, $\omega_p=0$. In this case the expressions for Q, D_0, and d_0 are

$$Q=\sqrt{I_s(r-1)}, \quad D_0=\frac{\kappa}{c}, \quad d_0=0, \tag{3.21}$$

where $r=R/R_{\mathrm{th}}$ is the dimensionless pumping rate, R_{th} is the threshold pumping rate, and I_s is the saturation intensity; the latter two are given by

$$R_{\mathrm{th}}=\frac{\gamma\kappa}{c}, \quad I_s=\frac{\gamma}{2c}. \tag{3.22}$$

The frequency detuning Δ in this case is $\Delta=-\kappa\alpha$, and the phase ψ is arbitrary. This phase determines the orientation of the linear polarization. We remind here that the linearly polarized field components $a_x(t)$ and $a_y(t)$ are related to the circularly polarized ones as

$$a_x(t)=\frac{a_+(t)+a_-(t)}{\sqrt{2}}, \quad a_y(t)=\frac{a_+(t)-a_-(t)}{\sqrt{2}i}. \tag{3.23}$$

These linearly polarized components for the stationary solution (3.21) are given by

$$a_x=\sqrt{2}Q\cos\psi, \quad a_y=\sqrt{2}Q\sin\psi. \tag{3.24}$$

It should be noted that the arbitrariness of the phase ψ results in the phase diffusion of the polarization of the light similar to the usual phase diffusion typical for the lasers.

When $\omega_p\neq 0$, there are in general four types of stationary solutions; two of them have linear polarization along the x and y axes, and two other have elliptical polarization. We shall consider here only linearly polarized solutions because only this type of behavior was observed in our experiments. For each of these solutions the phase anisotropy breaks the rotational invariance with respect to the polarization of the field and the phase ψ is no longer arbitrary. The x-polarized solution corresponds to $\psi_x=0$, and the y-polarized solution to $\psi_y=\pi/2$. For both types of solutions the values of Q, D_0, and d_0 are still given by Eq. (3.21). However, the frequency detunings Δ in Eq. (3.20) are different for these two solutions and equal to

$$\Delta_{x,y}=-(\kappa\alpha\pm\omega_p), \tag{3.25}$$

where the upper sign corresponds to the x-polarized solution and the lower sign to the y-polarized one.

The stability of these solutions has also been studied in detail in Ref. [6]. The x-polarized solution is stable for pumping rate r, such that

$$r<r_x=1+\frac{\gamma_s\omega_p}{\gamma(\kappa\alpha-\omega_p)}, \tag{3.26}$$

while the y-polarized solution is stable when

$$r>r_y=1-\frac{\gamma_s}{\gamma}+2\alpha\frac{\omega_p}{\gamma}. \tag{3.27}$$

As pointed out in Ref. [6], two curves $r_x(\omega_p)$ and $r_y(\omega_p)$ divide the r-ω_p plane into four different stability regions. In the first region, both x- and y-polarized solutions are stable, in the second both are unstable, in the third(fourth) only $x(y)$-polarized solution is stable. For more details we refer the reader to Ref. [6]. For low pumping rate only x-polarized solution is stable. Therefore, in this paper we restrict ourselves to analyzing the quantum fluctuations around this solution. More general investigation will be published elsewhere.

IV. SPECTRA OF THE QUANTUM FLUCTUATIONS

To calculate the quantum fluctuations around the stationary solution we shall linearize Eqs. (3.13)–(3.15) around the steady state given by Eq. (3.20). As mentioned above we shall consider here only x-polarized stationary solution. Adding small fluctuations to the stationary solutions we can write the field and atomic variables around the steady state as

$$a_\pm(t)=[Q+\delta a_\pm(t)]e^{i\Delta t}, \quad D(t)=D_0+\delta D(t),$$
$$d(t)=\delta d(t). \tag{4.1}$$

In this equation and in what follows we have dropped the index x in Δ_x since we shall be concerned only with x-polarized solution. Substituting these expressions into Eqs. (3.13)–(3.15) and linearizing, we arrive at the following equations for small fluctuations:

$$\frac{d}{dt}\delta a_\pm(t)=i\omega_p\delta a_\pm(t)-i\omega_p\delta a_\mp(t)+c(1-i\alpha)\times Q[\delta D(t)\pm\delta d(t)]+F_\pm(t)e^{-i\Delta t},$$

$$\frac{d}{dt}\delta D(t)=-(\gamma+2cQ^2)\delta D(t)-cQD_0[\delta a_+(t)+\delta a_-(t)+\mathrm{c.c.}]+F_D(t),$$

$$\frac{d}{dt}\delta d(t)=-(\gamma_s+2cQ^2)\delta d(t)-cQD_0[\delta a_+(t)-\delta a_-(t)+\mathrm{c.c.}]+F_d(t). \tag{4.2}$$

It is convenient to introduce the fluctuations of the linearly polarized components of the field, $\delta a_x(t)$ and $\delta a_y(t)$, defined according to Eq. (3.23), for which the set of coupled equations (4.2) decouples in two sets of independent equations for $\delta a_x(t)$ and $\delta a_y(t)$ with the Langevin forces $F_x(t)$ and $F_y(t)$ defined by the same Eq. (3.23). Moreover, we shall define the fluctuations of the amplitude and the phase quadrature components, $\delta X_x(t)$ and $\delta Y_x(t)$, of the x-polarized field component,

$$\delta X_x(t)=\frac{1}{2}[\delta a_x(t)+\delta a_x^*(t)],$$

$$\delta Y_x(t)=\frac{1}{2i}[\delta a_x(t)-\delta a_x^*(t)], \tag{4.3}$$

and similarly for the *y*-polarized component. For these fluctuations we obtain the following equations:

$$\frac{d}{dt}\delta X_x(t)=\sqrt{2}cQ\,\delta D(t)+R_x(t),$$

$$\frac{d}{dt}\delta Y_x(t)=-\sqrt{2}\alpha cQ\,\delta D(t)+S_x(t),$$

$$\frac{d}{dt}\delta D(t)=-\Gamma\,\delta D(t)-2\sqrt{2}\kappa Q\,\delta X_x(t)+F_D(t), \tag{4.4}$$

and

$$\frac{d}{dt}\delta X_y(t)=-2\omega_p\delta Y_y(t)-\sqrt{2}\alpha cQ\,\delta d(t)+R_y(t),$$

$$\frac{d}{dt}\delta Y_y(t)=2\omega_p\delta X_y(t)-\sqrt{2}cQ\,\delta d(t)+S_y(t),$$

$$\frac{d}{dt}\delta d(t)=-\Gamma_s\delta d(t)+2\sqrt{2}\kappa Q\,\delta Y_y(t)+F_d(t), \tag{4.5}$$

where the new Langevin forces $R_x(t)$ and $S_x(t)$ are defined as

$$R_x(t)=\frac{1}{2}[F_x(t)e^{-i\Delta t}+F_x^*(t)e^{i\Delta t}],$$

$$S_x(t)=\frac{1}{2i}[F_x(t)e^{-i\Delta t}-F_x^*(t)e^{i\Delta t}], \tag{4.6}$$

and similarly for $R_y(t)$ and $S_y(t)$. In Eqs. (4.4) and (4.5) we have introduced

$$\Gamma\equiv\gamma+2cQ^2=\gamma r,\quad \Gamma_s\equiv\gamma_s+2cQ^2=\gamma_s+\gamma(r-1), \tag{4.7}$$

and used the stationary solution $D_0=\kappa/c$.

To solve Eqs. (4.4) and (4.5) we take the Fourier transform of the field and atomic fluctuations,

$$\delta X_x(\Omega)=\frac{1}{\sqrt{2\pi}}\int_{-\infty}^{+\infty}\delta X_x(t)e^{i\Omega t}dt, \tag{4.8}$$

and similarly for all other variables that converts these differential equations into algebraic ones. After a simple algebra we obtain the following expressions for the fluctuations of the amplitude quadratures $\delta X_x(\Omega)$ and $\delta X_y(\Omega)$:

$$\delta X_x(\Omega)=\frac{1}{D_x(\Omega)}\{(\Gamma-i\Omega)R_x(\Omega)+\sqrt{2}cQF_D(\Omega)\}, \tag{4.9}$$

$$\delta X_y(\Omega)=\frac{1}{D_y(\Omega)}\{[2\kappa\gamma(r-1)-i\Omega(\Gamma_s-i\Omega)]R_y(\Omega)-[2\alpha\kappa\gamma(r-1)+2\omega_p(\Gamma_s-i\Omega)]S_y(\Omega)+\sqrt{2}cQ(2\omega_p+i\alpha\Omega)F_d(\Omega)\}, \tag{4.10}$$

with

$$D_x(\Omega)=-i\Omega(\Gamma-i\Omega)+2\kappa\gamma(r-1), \tag{4.11}$$

$$D_y(\Omega)=(\Gamma_s-i\Omega)(4\omega_p^2-\Omega^2)+2\kappa\gamma(r-1)(2\alpha\omega_p-i\Omega). \tag{4.12}$$

Using Eqs. (3.6)–(3.12) and Eqs. (3.17)–(3.19) we have calculated the correlation functions of the Langevin forces $R_\alpha(t),S_\alpha(t)$ with $\alpha=x,y$, and $F_D(t),F_d(t)$ for the stationary regime of VCSEL taking into account the stationary solutions (3.20). The nonzero correlation functions are given by

$$\begin{aligned}\langle R_x(t)R_x(t')\rangle&=\langle R_y(t)R_y(t')\rangle\\&=\langle S_x(t)S_x(t')\rangle\\&=\langle S_y(t)S_y(t')\rangle\\&=\kappa\delta(t-t'),\end{aligned} \tag{4.13}$$

$$\langle F_D(t)F_D(t')\rangle=\frac{\kappa}{c}\Gamma\left(1-\frac{1}{2}p\right)\delta(t-t'), \tag{4.14}$$

$$\langle F_d(t)F_d(t')\rangle=\frac{\kappa}{c}\Gamma_s\delta(t-t'), \tag{4.15}$$

$$\langle F_D(t)R_x(t')\rangle=\langle F_d(t)S_y(t')\rangle=2\kappa Q\,\delta(t-t'). \tag{4.16}$$

Equations (4.9)–(4.12) together with correlation functions (4.13)–(4.16) allow us to evaluate an arbitrary correlation function of the laser light emitted by the VCSEL. It this paper we shall investigate the intensity fluctuations of different polarization components of the laser light emitted by the VCSEL. Experimentally, these fluctuations can be measured by photodetecting the light emitted by the VCSEL after this light has passed through a polarizer, which selects a particular polarization component of the electromagnetic wave [11]. The most general unitary polarization vectors $\vec{e}_p$, $p=1,2$, selected by a polarizer, can be written as

$$\vec{e}_1=\vec{e}_x\cos\varphi-e^{-i\delta}\vec{e}_y\sin\varphi,$$

$$\vec{e}_2=\vec{e}_x\sin\varphi+e^{-i\delta}\vec{e}_y\cos\varphi. \tag{4.17}$$

These unitary polarization vectors satisfy the condition $\vec{e}_p\cdot\vec{e}_q^{\,*}=\delta_{pq}$. For simplicity we shall consider $\delta=0$. Experimentally, this situation can be realized in a setup consisting

of a $\lambda/2$ wave plate and a beam splitter, shown in Fig. 11. Variation of the angle φ is obtained by turning the $\lambda/2$ wave plate.

After passing through the polarizer the vector $\vec{E}(t)$ of the electromagnetic field is projected into the polarization vector $\vec{e}_p$ as $a_p(t)=\vec{E}(t)\cdot\vec{e}_p$. Writing the electromagnetic field $\vec{E}(t)$ in terms of the *x*- and *y*-polarized components,

$$\vec{E}(t)=a_x(t)\vec{e}_x+a_y(t)\vec{e}_y, \tag{4.18}$$

and using Eq. (4.17), we obtain the following relations between the field amplitudes $a_p(t)$, $a_x(t)$, and $a_y(t)$:

$$a_1(t)=a_x(t)\cos\varphi-a_y(t)\sin\varphi,$$

$$a_2(t)=a_x(t)\sin\varphi+a_y(t)\cos\varphi. \tag{4.19}$$

After selection of a particular polarization component of the electromagnetic wave determined by the amplitude $a_p(t)$, the light is photodetected and one observes the photocurrent fluctuation spectrum $(\delta i_p^2)_\Omega$ defined as

$$(\delta i_p^2)_\Omega=\int_{-\infty}^{+\infty}dt e^{i\Omega t}\langle\delta i_p(0)\,\delta i_p(t)\rangle, \tag{4.20}$$

where $\langle\delta i_p(0)\,\delta i_p(t)\rangle$ is the correlation function of the photocurrent fluctuations $\delta i_p(t)=i_p-\langle i_p\rangle$, and $\langle i_p\rangle$ is the mean value of the photocurrent, $\langle i_p\rangle=\eta c\langle a_p^\dagger a_p\rangle$; here η is the quantum efficiency of photodetector, which we shall consider to be unity, and c is the light velocity.

Following Ref. [24] the photocurrent fluctuation spectrum can be expressed through the fluctuation spectrum of the amplitude quadrature component of the field inside the laser cavity. We shall define the fluctuations of the amplitude and phase quadratures of the field with polarization component $a_p(t)$,

$$\delta X_p(\Omega)=\frac{1}{2}[\delta a_p(\Omega)+\delta a_p^*(-\Omega)],$$

$$\delta Y_p(\Omega)=\frac{1}{2i}[\delta a_p(\Omega)-\delta a_p^*(-\Omega)]. \tag{4.21}$$

The spectral correlation functions of these quadratures are δ correlated:

$$\langle\delta X_p(\Omega)\,\delta X_p(\Omega')\rangle=(\delta X_p^2)_\Omega\delta(\Omega+\Omega'),$$

$$\langle\delta Y_p(\Omega)\,\delta Y_p(\Omega')\rangle=(\delta Y_p^2)_\Omega\delta(\Omega+\Omega'),$$

$$\langle\delta X_p(\Omega)\,\delta Y_p(\Omega')\rangle=(\delta X_p\delta Y_p)_\Omega\delta(\Omega+\Omega'), \tag{4.22}$$

with $(\delta X_p^2)_\Omega$ and $(\delta Y_p^2)_\Omega$ being the spectral densities of the corresponding quadratures, and $(\delta X_p\delta Y_p)_\Omega$ their cross-spectral density. In this paper, we have calculated these spectral densities numerically. The analytical calculations are in progress and we shall publish them elsewhere.

The photocurrent fluctuation spectrum $(\delta i_p^2)_\Omega$ normalized to the shot-noise level given by $(\delta i_p^2)_\Omega=\langle i_p\rangle$, is related to the spectral density of the amplitude quadrature component as

$$(\delta i_p^2)_\Omega/\langle i_p\rangle=1+8\kappa(\delta X_p^2)_\Omega. \tag{4.23}$$

To calculate the photocurrent fluctuation spectrum (4.23) we have expressed the spectral densities $(\delta X_p^2)_\Omega$ through the spectral densities of the *x*- and *y*-polarized amplitude quadrature components, $(\delta X_x^2)_\Omega$, $(\delta X_y^2)_\Omega$, and their cross-spectral density $(\delta X_x\delta X_y)_\Omega$ using Eqs. (4.19) and (4.21). The results are significantly simplified by the fact that, as follows from our calculations, the latter cross-spectral density turns out to be zero, $(\delta X_x\delta X_y)_\Omega=0$. Thus we obtain the following expressions for the photocurrent fluctuation spectra $(\delta i_1^2)_\Omega$ and $(\delta i_2^2)_\Omega$:

$$(\delta i_1^2)_\Omega\langle i_1\rangle=1+8\kappa[\cos^2\varphi(\delta X_x^2)_\Omega+\sin^2\varphi(\delta X_y^2)_\Omega], \tag{4.24}$$

$$(\delta i_2^2)_\Omega\langle i_2\rangle=1+8\kappa[\sin^2\varphi(\delta X_x^2)_\Omega+\cos^2\varphi(\delta X_y^2)_\Omega]. \tag{4.25}$$

We have also calculated the cross-correlation spectrum of the photocurrent fluctuations for two orthogonal polarization components $\vec{e}_1$ and $\vec{e}_2$ defined as

$$C_{12}(\Omega)=\frac{(\delta i_1\delta i_2)_\Omega}{\sqrt{(\delta i_1^2)_\Omega(\delta i_2^2)_\Omega}}. \tag{4.26}$$

This spectrum is normalized as $|C_{12}(\Omega)|\leqslant 1$, and $C_{12}(\Omega)=-1$ corresponds to perfect anticorrelations while $C_{12}(\Omega)=1$ to perfect correlations. Experimentally, this spectrum can be measured as

$$C_{12}(\Omega)=\frac{(\delta i^2)_\Omega-(\delta i_1^2)_\Omega-(\delta i_2^2)_\Omega}{2\sqrt{(\delta i_1^2)_\Omega(\delta i_2^2)_\Omega}}, \tag{4.27}$$

where $(\delta i^2)_\Omega$ is the fluctuation spectrum of the total photocurrent $i(t)=i_1(t)+i_2(t)$.

It can be easily shown that this cross-correlation spectrum expressed in terms of the spectral densities of the *x*- and *y*-polarized amplitude quadrature components, $(\delta X_x^2)_\Omega$, $(\delta X_y^2)_\Omega$, reads

$$C_{12}(\Omega)=\frac{8\kappa\sin\varphi\cos\varphi[(\delta X_x^2)_\Omega-(\delta X_y^2)_\Omega]}{\sqrt{(1+8\kappa[\cos^2\varphi(\delta X_x^2)_\Omega+\sin^2\varphi(\delta X_y^2)_\Omega])(1+8\kappa[\sin^2\varphi(\delta X_x^2)_\Omega+\cos^2\varphi(\delta X_y^2)_\Omega])}}. \tag{4.28}$$

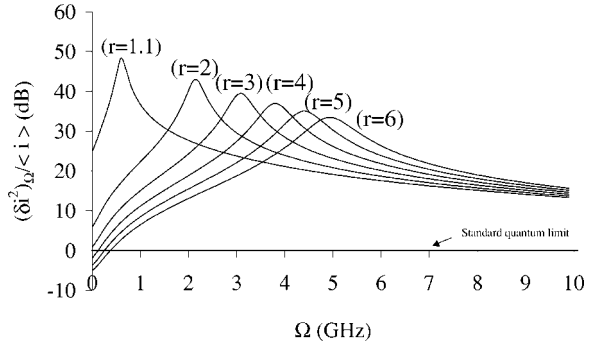

FIG. 2. Normalized photocurrent noise spectra $(\delta i^2)_\Omega / \langle i \rangle$(dB) of the total beam for different pump parameters r and regular pumping $p=1$. The values of other parameters are $\kappa=100$ GHz, $\gamma=1$ GHz, $\gamma_\perp=1000$ GHz, $\gamma_s=50$ GHz, $\omega_p=40$GHz, and $\alpha=3$. The standard quantum limit corresponds to $(\delta i^2)_\Omega / \langle i \rangle = 0$ dB.

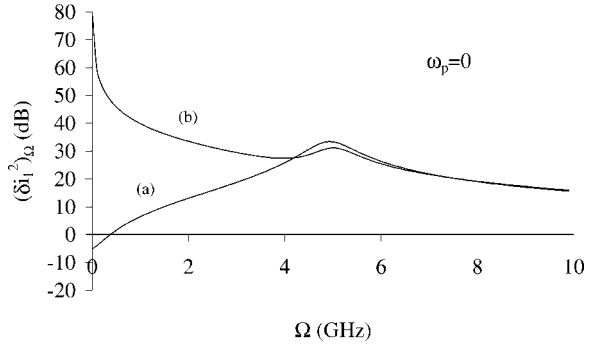

FIG. 3. Photocurrent noise spectra $(\delta i^2)_\Omega$ of the total beam (curve *a*) and $(\delta i_1^2)_\Omega$ of the $\varphi=45°$ polarization component (curve *b*) for $r=6$, $p=1$, without birefringence, $\omega_p=0$. All other parameters are as in Fig. 2.

Note that measuring experimentally the cross-correlation spectrum (4.28) and one of the spectra (4.24) for a fixed value of the angle φ different from $\varphi=0,\pi/2$ we can deduce both spectral densities $(\delta X_x^2)_\Omega, (\delta X_y^2)_\Omega$.

V. THEORETICAL PREDICTIONS

In this section we shall present several curves of the fluctuation spectra calculated theoretically from our quantum model. In the following section we shall compare some of these curves with the experimental observations. In Fig. 2 we have plotted a set of photocurrent noise spectra $(\delta i^2)_\Omega$ of the total photocurrent for the regular pump $p=1$, at different pump rates r. These spectra can be observed experimentally by photodetection of the total light beam, i.e., without the polarizer. Theoretically, they are obtained by putting the angle $\varphi=0$ in Eq. (4.24),

$$(\delta i^2)_\Omega / \langle i \rangle = (\delta i_1^2)_\Omega / \langle i_1 \rangle_{\varphi=0} = 1 + 8\kappa (\delta X_x^2)_\Omega . \quad (5.1)$$

The cavity decay rate κ and the population decay rate γ are calculated from the data given to us by the group of the University of Ulm that has fabricated and provided us with the samples. The other parameters, namely, $\gamma_\perp, \gamma_s, \omega_p$, and α are taken from the literature. For example, for γ_s we use the values given in Refs. [27,28]. For these values the x-polarized solution is stable for $r<6.5$, while the y-polarized solution is stable for $r>131$. The spectra plotted in Fig. 2 are analogous to those obtained with the usual two-level systems [24]. They are dominated by a large excess noise at the relaxation oscillations frequency. For regular pumping $p=1$, and high pump rate r, the model predicts squeezing at low frequencies. Indeed, the intensity fluctuations are only coupled to the fluctuation of the total population, which is regularly pumped.

We turn now to investigation of the photocurrent noise spectrum $(\delta i_1^2)_\Omega$ for the light passed through a rotatable polarizer oriented at the angle φ to the polarization of the laser light. As follows from Eq. (4.24) the spectral density $(\delta X_1^2)_\Omega$ of the amplitude quadrature component after polarization is given by the sum of spectral densities of the x- and y-polarized amplitude quadratures $(\delta X_x^2)_\Omega$ and $(\delta X_y^2)_\Omega$ with corresponding transmission coefficients depending on the angle φ. This result is equivalent to an interference experiment with two independent light waves passing through a beam splitter with the transmission and reflection coefficients given by $\cos\varphi$ and $\sin\varphi$.

In the case of a single-mode laser linearly polarized along the x axis, the spectral density of the y-polarized component is equal to zero, $(\delta X_y^2)_\Omega = 0$, since it corresponds to the vacuum state of this polarization component. Equation (4.24) is applicable to this case as well with the vanishing term proportional to $(\delta X_y^2)_\Omega$. The difference of VCSELs is that, as demonstrated by our calculations, the contribution from the fluctuations of the y-polarized component is not zero and has to be taken into account for correct description of the fluctuation properties of the laser light. In spite of the fact that the mean amplitude of the y-polarized field component is zero, it gives the contribution to the photocurrent noise spectrum $(\delta i_1^2)_\Omega$ due to the interference of fluctuations of this component with the nonzero field amplitude of the x-polarized component. The situation is similar to the homodyne detection with the x-polarized field component playing the role of the local oscillator.

Let us now consider the effect of the birefringence ω_p on the photocurrent noise spectra. The birefringence has no influence on the photocurrent noise of the total laser beam. Indeed, as follows from Eq. (5.1) the photocurrent noise spectrum $(\delta i^2)_\Omega$ is related to the spectral density of the x-polarized amplitude quadrature $(\delta X_x^2)_\Omega$. In turn, we observe from Eqs. (4.9),(4.11) and (4.13)–(4.16) that this spectral density is independent of ω_p. On the contrary, the role of the birefringence is very important in the photocurrent noise spectrum $(\delta i_1^2)_\Omega$ of the light passed through the polarizer.

Putting $\omega_p=0$ in Eq. (4.12), we obtain $i\Omega$ as a factor in this denominator, which gives a divergence at low frequencies in the spectral density $(\delta X_y^2)_\Omega$ of the y-polarized component. Since this spectral density appears in the photocurrent noise spectrum $(\delta i_1^2)_\Omega$, the spectrum also diverges at low frequencies. This is illustrated in Fig. 3, where we have plotted the photocurrent noise spectra of the polarization

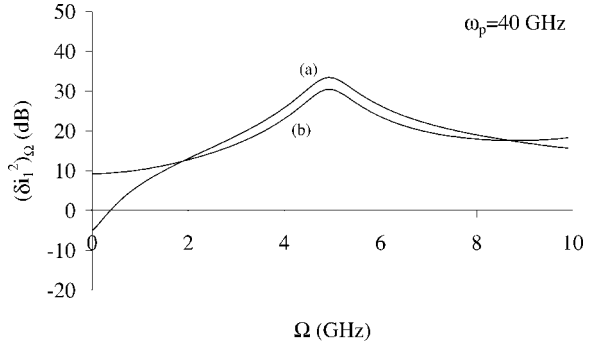

FIG. 4. Photocurrent noise spectra $(\delta i^2)_\Omega$ of the total beam (curve *a*) and $(\delta i_1^2)_\Omega$ of the $\varphi=45°$ polarization component (curve *b*) for $r=6$, $p=1$, and birefringence equal to $\omega_p=40$ GHz. All other parameters as in Fig. 2.

component $\vec{e}_1$ for $\varphi=\pi/4$ and of the total beam. We notice that the photocurrent noise of the polarization component tends to infinity as the frequency Ω approaches zero. This result is easily understood if we remember that the phase ψ in the stationary solution without birefringence is not determined and remains arbitrary. It experiences the phase diffusion as the optical phase in usual single-mode lasers [24] with typical diverging behavior at zero frequency.

If $\omega_p \neq 0$, the phase ψ is no longer arbitrary. For the *x*-polarized solution it is $\psi=0$. Respectively, there is no phase diffusion related to the phase ψ, and the fluctuations at low frequencies in the photocurrent spectrum remain finite. In Fig. 4, we have plotted the photocurrent noise spectrum $(\delta i_1^2)_\Omega$ at $\varphi=\pi/4$ for the same parameters as in Fig. 3 except the birefringence $\omega_p=40$ GHz. As expected, the large excess noise at low frequencies is suppressed.

In Fig. 5 we have given the photocurrent noise spectrum $(\delta i_1^2)_\Omega$ at a fixed frequency $\Omega=10$ MHz as a function of the polarization angle φ for the pumping rate $r=1.85$. In the same figure we have shown the value of the shot noise of the filtered VCSEL beam and the photocurrent noise of a laser beam polarized along *x* axis and filtered by a polarizer. The

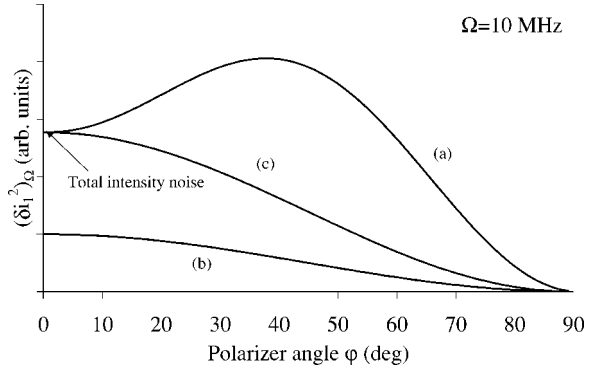

FIG. 5. Photocurrent noise $(\delta i_1^2)_\Omega$ at $\Omega=10$ MHz of the beam filtered by a polarizer versus the angle φ (a), the shot-noise level of the filtered beam at the same frequency (b), and the photocurrent noise of a *single-polarization-mode* filtered beam having the same intensity noise as the VCSEL beam (c). Pump parameter $r=1.85$. All other parameters are as in Fig. 2.

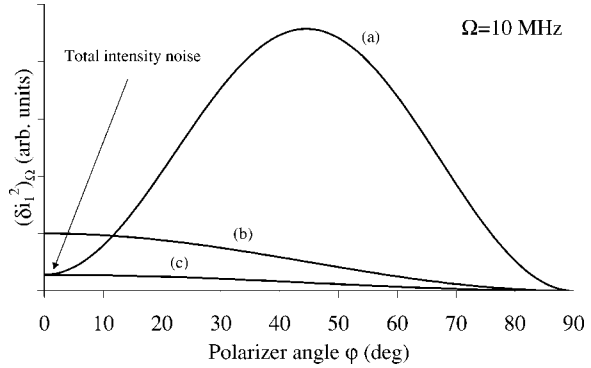

FIG. 6. Same curves as in Fig. 5 but for higher pumping rate $r=6$.

results of Fig. 5 confirm that the VCSEL beam cannot be considered as a laser beam polarized along the *x* axis as far as the photocurrent noise is concerned. Owing to the interference of quantum fluctuations of the subthreshold *y*-polarized component with the *x*-polarized field amplitude, the photocurrent fluctuations for intermediate positions of the polarizer are higher than fluctuations of a corresponding *x*-polarized beam. This effect is even more pronounced for higher pumping rates as illustrated in Fig. 6 where we have taken $r=6$.

The increase of the photocurrent noise at intermediate values of φ can be easily understood with our model. Indeed, Eq. (4.24) gives, for example, for $\varphi=\pi/4$,

$$(\delta i_1^2)_\Omega / \langle i_1 \rangle_{\varphi=\pi/4} = 1 + 4\kappa[(\delta X_x^2)_\Omega + (\delta X_y^2)_\Omega]. \quad (5.2)$$

Therefore, for $(\delta X_y^2)_\Omega > (\delta X_x^2)_\Omega$ the photocurrent noise after polarization is higher than the noise of the total beam.

We have already seen that the amplitude correlations between the *x*-polarized and *y*-polarized components are equal to zero. However, for orthogonally polarized components $\vec{e}_1$ and $\vec{e}_2$ these correlations can reach very high values. In Fig. 7 we have plotted the cross-correlation function $C_{12}(\Omega)$ for $\varphi=\pi/4$ as a function of the frequency Ω. At low frequencies the total intensity noise is 72% below the shot noise due to the regular pumping. The two photocurrents i_1 and i_2 at $\varphi=\pi/4$ are strongly anticorrelated and C_{12} is close to -1. At higher frequencies the total intensity noise is very high above

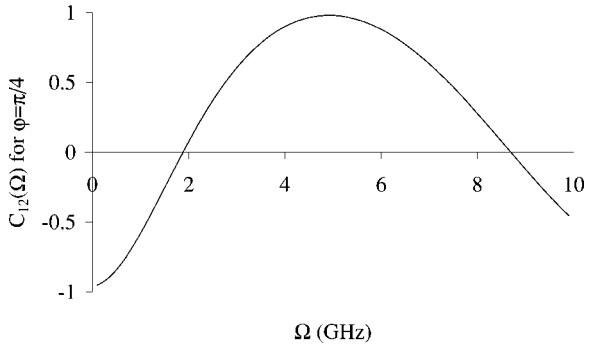

FIG. 7. Cross-correlation spectrum $C_{12}(\Omega)$ for $\varphi=\pi/4$. All parameters as in Fig. 4.

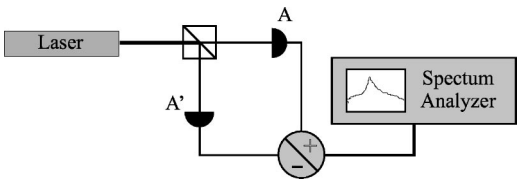

FIG. 8. Correlated beams obtained with a beam splitter.

the shot noise, especially near the frequency of the relaxation oscillations. The two polarization components present very large classical noise and are strongly correlated with C_{12} close to 1. This situation is similar to the case of two optical beams with large excess noise after a 50/50 beam splitter (see Fig. 8). Since for large excess noise we can neglect the shot noise of the total photocurrent, the photocurrent difference $I_A - I_{A'}$ is very small while the sum $I_A + I_{A'}$ gives the intensity noise of the total beam. This means that the beams A and A' are strongly correlated.

Finally, in Fig. 9 we consider the variation of the cross correlations C_{12} at a fixed frequency $\Omega = 10$ MHz with the angle φ. We observe from Fig. 9 that for $\varphi = \pi/4$ the two polarizations components are strongly anticorrelated with $C_{12} = -68\%$. At the same time these two polarization components have a large excess noise of 738% above the shot-noise level.

In the following section we shall compare our theoretical predictions with the experimental results obtained for the high-quality VCSELs.

VI. EXPERIMENTAL RESULTS

We use oxide-confined VCSELs (made at the Department of Optoelectronics of the University of Ulm) with different active media diameters, 3–20 μm. The devices are schematically represented in Fig. 10. They consist of carbon-doped p-type AlGaAs/AlGaAs and silicon-doped n-type AlAs/AlGaAs Bragg reflectors with pairs of quarter wavelength thick layers. The top (bottom) mirror has a reflectivity of 99.8% (99%). They are coated on each side by a cladding layer containing the three active 8 nm-thick GaAs quantum wells. The emission wavelength is about 840 nm. The oxide aperture provides both current and optical confinements. The devices are attached to a copper plate using silver paste.

We take advantage of the principle of pump-noise suppression to minimize the noise in the laser output. For this

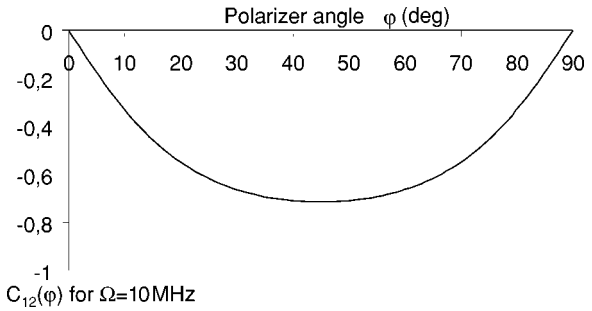

FIG. 9. Cross-correlations C_{12} at $\Omega = 10$ MHz vs the angle φ. All parameters are as in Fig. 4.

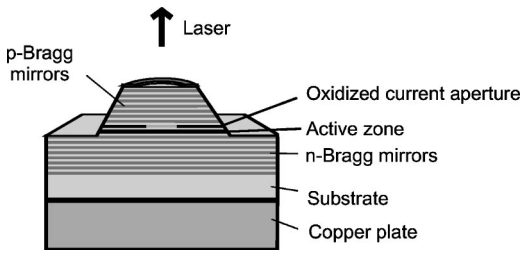

FIG. 10. Schematic representation of the VCSEL.

purpose, a homemade low-noise power supply with an appropriate LC filter provides the regular electrical current that drives the VCSELs. The VCSELs are also thermally stabilized with an active temperature stabilization. With this stabilization, we were able to operate at a fixed temperature with a drift as small as 0.01 °C/h. The emitted beam is collimated by an antireflection coated microscope objective located at a distance of 2 mm from the laser output. This objective has a large numerical aperture (= 0.6) to avoid optical losses that would deteriorate the squeezing. To measure the intensity noise and the corresponding shot noise, the standard scheme consists of a polarizing beam splitter that separates the beam emitted by the laser into two equal parts that are detected by means of high quantum efficiency balanced photodiodes. The sum of the two photocurrents is proportional to the intensity noise of the total beam while the difference is proportional to the corresponding shot noise [29]. However, in our case it is better to use only one photodiode (FND100, bandwidth 1–20 MHz, and quantum efficiency of 90%). Indeed, because of the multimode operation with two orthogonal linear polarizations, the shot noise obtained with a balanced detection would not be reliable. For this reason we preferred to use a separately calibrated shot noise. The shot-noise reference is obtained by a balanced detection of a standard, edge-emitting laser diode beam that has an intensity noise less than 1 dB above the shot-noise level in the range of frequencies of 1–20 MHz. We carefully checked the linear dependence of the calibrated shot-noise signal with the optical power incident on the photodiodes. The shot noise obtained with this method was in agreement within 0.1 dB with the value obtained from a thermal light generating the same dc current on the photodiode. The photodiode is connected via a low-noise homemade amplifier (with a CLC425) and electronic amplifier (Nucletude 4-40-1A) to a spectrum analyzer (Tektronics 2753P). With this

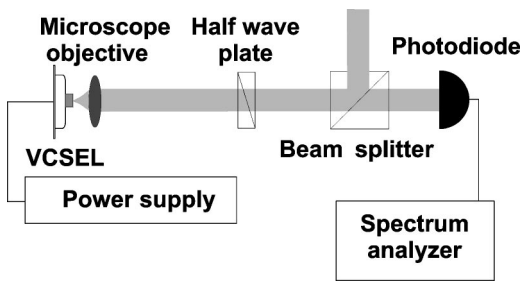

FIG. 11. Experimental setup to measure the intensity noise of the polarization components.

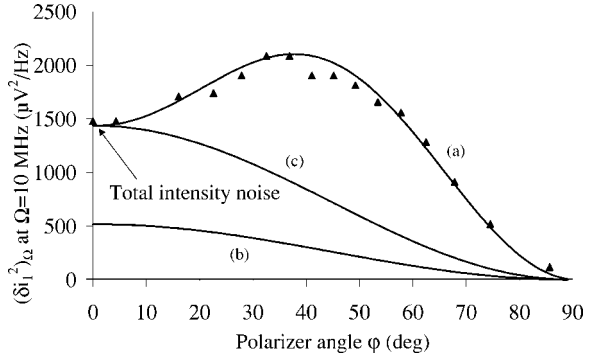

FIG. 12. Photocurrent noise spectrum $(\delta i_1^2)_\Omega$ vs the angle φ. Experimental results are shown by black triangles; curve (a) corresponds to the theoretical predictions, curve (b) gives the shot noise of the filtered beam, and curve (c) the noise of a single-polarization-mode filtered beam having the same intensity noise as the VCSEL beam. The values of the parameters are $\kappa=100$ GHz, $\gamma=1$ GHz, $\gamma_\perp=1000$ GHz, $\gamma_s=50$ GHz, $\omega_p=40$ GHz, $\alpha=3$, $r=1.85$, and $\Omega=10$ MHz at $p=1$.

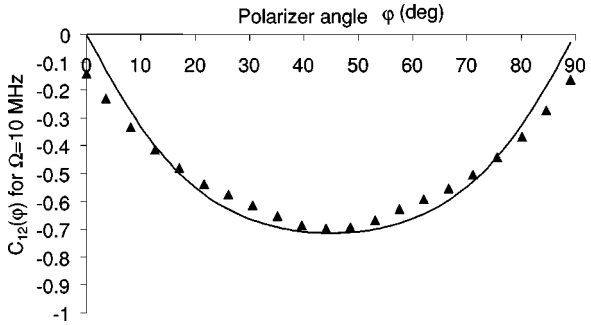

FIG. 13. Cross-correlations C_{12} at $\Omega=10$ MHz vs the angle φ. Experimental results are shown by black triangles, solid curve corresponds to the theoretical predictions. The values of the parameter are the same as in Fig. 12.

setup the electronic noise was more than 6 dB below the signal for a typical detected power of 1.5 mW. In our experiment we could also perform a spectral analysis of the laser beam with a high-resolution monochromator (0.03 nm at 840 nm). At the output of the monochromator, the relative powers of the individual transverse modes are measured with a photodetector and their polarizations are determined using a Glan polarizer (extinction ratio 10^{-4}).

To measure the intensity noise of the polarization components we use a half-wave plate and a beam splitter (see Fig. 11). In the following, the measured intensity noise is corrected for optical losses.

Our VCSELs have a mean quantum efficiency of 50% and a threshold of 1 mA. For all samples the first mode above threshold is the linearly polarized TEM_{00} mode. When the driving current is increased, other transverse modes start to oscillate. At pump rates higher than $r=2$ the VCSELs always operate with several transverse modes above threshold. Since squeezing is predicted theoretically for pump rates higher than $r=2$ we were not able to obtain squeezing in a single-mode operation. At very high pump rates the laser beam is composed of transverse modes having the same transverse intensity distributions but orthogonal linear polarization. In this case we can evaluate the birefringence ω_p by measuring the optical frequency shift between the orthogonally polarized modes. This frequency shift is found to be 80 GHz, which gives $\omega_p=40$ GHz.

For our most recent samples, in single-mode operation, the intensity noise measured in the direction orthogonal to the polarization of the lasing mode is very weak (close to the electronic dark noise). Even if our VCSELs do not exhibit squeezing in a single-mode operation, the intensity noise of the lasing mode is very close to the standard quantum limit where quantum effects become important. Therefore, to take into account these quantum effects we have developed a full quantum model. In this case we expect a good agreement between the predictions of our model and the experimental results. In Fig. 12 we have shown the results obtained for a pump rate $r=1.85$. To compare our experimental results with theoretical predictions, we adjust the shot noise at $\varphi=0$ to the calculated shot-noise level. This corresponds to a normalization of all our curves and leaves no adjustable free parameters. In Fig. 12 we notice a very good agreement between the theoretical predictions and the experimental results.

We have also measured the cross-correlations C_{12} at $\Omega=10$ MHz between orthogonal polarization components as a function of the angle φ of the polarizer (see Fig. 13). Once more, the agreement is very good. Moreover, our experimental results confirm that the *x*- *y*-polarized components are not correlated.

All these results confirm experimentally that the VCSELs cannot be considered as single-polarization-mode lasers. On one side, the intensity noise of the total beam is equal to the noise of the *x*-polarized component and the quantum fluctuations of the *y*-polarized component are not detectable. However, for the $\varphi=\pi/4$ polarized component we obtain both theoretically and experimentally an excess noise greater than the noise of the total beam. This result cannot be explained without taking into account the fluctuations of the subthreshold *y*-polarized component of the laser light.

VII. CONCLUSION

In conclusion, we have presented a full quantum model for VCSELs operating with one linearly polarized transverse mode above threshold driven by a sub-shot-noise electrical current. This model allows us to calculate the photocurrent noise for photodetection of the total laser beam and of the beam passed through a polarizer oriented at some arbitrary angle to the polarization of the laser light. We demonstrate that as far as the photocurrent noise is concerned, VCSELs cannot be considered as single-polarization-mode lasers. Namely, the quantum fluctuations of the nonlasing mode with polarization component orthogonal to that of the lasing mode must be taken into account. When the beam is filtered by a polarizer, the fluctuations of this subthreshold field component interfere with the field amplitude of the lasing mode and the intensity noise of the filtered beam may become higher than the total intensity noise. We also demonstrate that two orthogonally polarized components of the beam after the polarization can be strongly anticorrelated.

Our experimental results confirm the theoretical predictions of our model for VCSELs having an intensity noise of the lasing mode very close to the standard quantum limit. Our model could also be used for VCSELs exhibiting intensity noise squeezing in a single-mode operation. We have observed the increase of the intensity noise in the beam after the polarization over the intensity noise of the total beam. We have also confirmed experimentally the predictions concerning the anticorrelations between the two orthogonal polarization components. These characteristics are analogous to the anticorrelations observed in the multimode operation, which are capable of producing squeezing [4,20] and transverse spatial structures [30,31].

ACKNOWLEDGMENTS

We acknowledge support from the European project (VISTA): http://www.physics.ucc.ie/Vista2. We thank Yuri M. Golubev of St. Petersburg University, St. Petersburg (Russia) for all the interesting discussions we had and all of his remarks about our work. We also thank P. Schnitzer, R. Michalzik, and K. J. Ebeling of the University of Ulm, Ulm (Germany) for kindly providing the oxide-confined VCSELs.

[1] Y.M. Golubev and I.V. Sokolov, Zh. Eksp. Teor. Fiz. **87**, 408 (1984) [Sov. Phys. JETP **60**, 234 (1984)].
[2] Y. Yamamoto, S. Machida, and O. Nilsson, Phys. Rev. A **34**, 4025 (1986).
[3] C. Degen, J.L. Vey, W. ElsäBer, P. Schnitzer, and K.J. Ebeling, Electron. Lett. **34**, 1585 (1998).
[4] J.P. Hermier, A. Bramati, A.Z. Khoury, V. Josse, E. Giacobino, P. Schnitzer, R. Michalzik, and K.J. Ebeling, IEEE J. Quantum Electron. **37**, 87 (2001).
[5] P. Schnitzer, M. Grabherr, R. Jager, F. Mederer, R. Michalzik, D. Wiedenmann, and K.J. Ebeling, IEEE Photonics Technol. Lett. **11**, 769 (1999).
[6] J. Martin-Regalado, F. Prati, M. San Miguel, and N.B. Abraham, IEEE J. Quantum Electron. **33**, 765 (1997).
[7] J. Martin-Regalado, S. Balle, and M. San Miguel, Opt. Lett. **22**, 460 (1997).
[8] C.J. Chang-Hasnain, J.P. Harbison, L.T. Florez, and N.G. Stoffel, Electron. Lett. **27**, 163 (1991).
[9] K.D. Choquette, R.P. Schneider, K.L. Lear, and R.E. Leibenguth, IEEE J. Sel. Top. Quantum Electron. **1**, 661 (1995).
[10] J. Martin-Regalado, J.L.A. Chilla, J.J. Rocca, and P. Brusenbach, Appl. Phys. Lett. **70**, 3350 (1997).
[11] M.P. van Exter, M.B. Willemsen, and J.P. Woerdman, Phys. Rev. A **58**, 4191 (1998).
[12] M.B. Willemsen, M.P. van Exter, and J.P. Woerdman, Phys. Rev. A **60**, 4105 (1999).
[13] M. P. van Exter, M. B. Willemsen, and J. P. Woerdman, J. Opt. B: Quantum Semiclassical Opt. 637 (1999).
[14] F. Marin, A. Bramati, and E. Giacobino, Phys. Rev. Lett. **75**, 4606 (1995).
[15] S. Inoue, S. Machida, Y. Yamamoto, and H. Ohzu, Phys. Rev. A **46**, 2757 (1992).
[16] H. Wang, M.J. Freeman, and D.G. Steel, Phys. Rev. Lett. **71**, 3951 (1993).
[17] J.L. Vey and W. ElsäBer, Opt. Lett. **23**, 721 (1998).
[18] J.L. Vey, C. Degen, K. Auen, and W. ElsäBer, Phys. Rev. A **60**, 3284 (1999).
[19] E. Goobar, J.W. Scott, B. Thibeault, G. Robinson, Y. Akulova, and L.A. Coldren, Appl. Phys. Lett. **67**, 3697 (1995).
[20] D.C. Kilper, P.A. Roos, and J.L. Carlsten, Phys. Rev. A **55**, R3323 (1997).
[21] M. San Miguel, Q. Feng, and J.V. Moloney, Phys. Rev. A **52**, 1728 (1995).
[22] W. W. Chow, S. W. Koch, and M. Sargent, Jr., *Semiconductor-Laser Physics* (Springer-Verlag, Berlin, 1994).
[23] C. Benkert, M.O. Scully, J. Bergou, L. Davidovich, M. Hillery, and M. Orszag, Phys. Rev. A **41**, 2756 (1990).
[24] M.I. Kolobov, L. Davidovich, E. Giacobino, and C. Fabre, Phys. Rev. A **47**, 1431 (1993).
[25] L. Davidovich, Rev. Mod. Phys. **68**, 127 (1996).
[26] A. Bramati, V. Jost, F. Marin, and E. Giacobino, J. Mod. Opt. **44**, 1929 (1997).
[27] T.C. Damen, L. Vina, J.E. Cunningham, J. Shah, and L.J. Sham, Phys. Rev. Lett. **67**, 3432 (1991).
[28] S. Bar-Ad and I. Bar-Joseph, Phys. Rev. Lett. **68**, 349 (1992).
[29] T.C. Zhang, J.-Ph. Poizat, P. Grelu, J.-F. Roch, Ph. Grangier, F. Marin, A. Bramati, V. Jost, M.D. Levenson, and E. Giacobino, Quantum Semiclassic. Opt. **7**, 601 (1995).
[30] A. Bramati, J.P. Hermier, A.Z. Khoury, E. Giacobino, P. Schnitzer, R. Michalzik, K.J. Ebeling, J.-Ph. Poizat, and Ph. Grangier, Opt. Lett. **24**, 893 (1999).
[31] J.P. Hermier, A. Bramati, A.Z. Khoury, E. Giacobino, J.Ph. Poizat, T.J. Chang, and Ph. Grangier, J. Opt. Soc. Am. B **16**, 2140 (1999).